Short Article

Cell Stem Cell

Zika Virus Disrupts Neural Progenitor Development and Leads to Microcephaly in Mice

Graphical Abstract

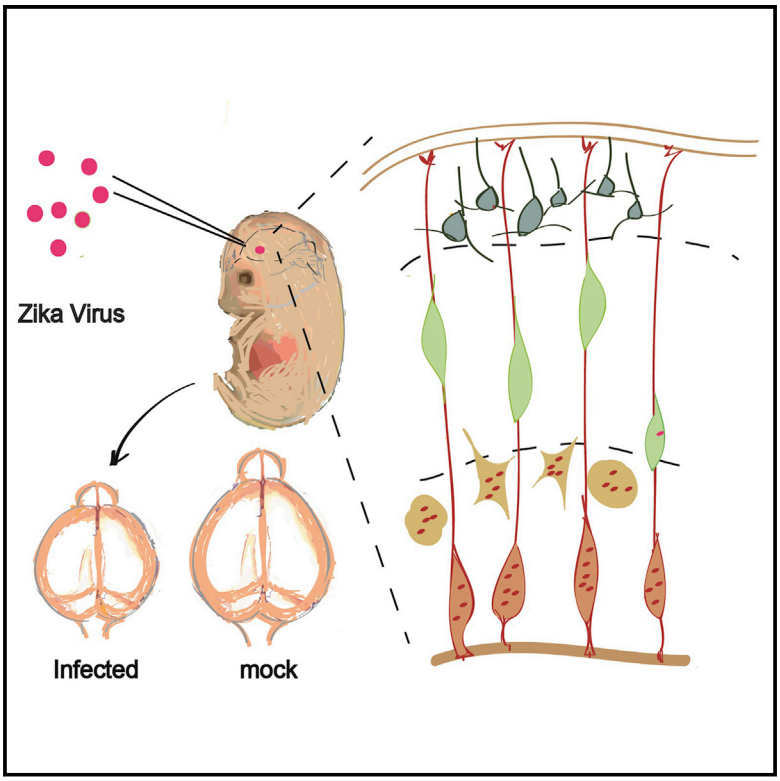

Authors

Cui Li, Dan Xu, Qing Ye, ..., Lei Shi, Cheng-Feng Qin, Zhiheng Xu

Correspondence

qincf@bmi.ac.cn (C.-F.Q.), zhxu@genetics.ac.cn (Z.X.)

In Brief

The suspected link between Zika virus (ZIKV) infection and microcephaly has raised urgent global alarm. However, there is so far no direct evidence for ZIKV infection impacting brain development. In this study, Li, Xu, and colleagues show that ZIKV replicates efficiently in the mouse embryonic brain by mainly targeting neural progenitor cells. They also show that infected brains are smaller with enlarged ventricles and a thinner cortex, consistent with a microcephalic phenotype.

Highlights

- Zika virus (ZIKV) replicates very efficiently in embryonic mouse brain
- ZIKV infects neural progenitor cells (NPCs) and causes microcephaly
- ZIKV infection leads to NPC cell-cycle arrest and defects in differentiation
- ZIKV infection induces immune response in brain and apoptosis of post-mitotic neurons

Li et al., 2016, Cell Stem Cell *19*, 1–7
July 7, 2016
http://dx.doi.org/10.1016/j.stem.2016.04.017

CellPress

Please cite this article in press as: Li et al., Zika Virus Disrupts Neural Progenitor Development and Leads to Microcephaly in Mice, Cell Stem Cell (2016), http://dx.doi.org/10.1016/j.stem.2016.04.017

Cell Stem Cell
Short Article

Zika Virus Disrupts Neural Progenitor Development and Leads to Microcephaly in Mice

Cui Li,[1,2,7] Dan Xu,[5,7] Qing Ye,[3,7] Shuai Hong,[1,2,7] Yisheng Jiang,[1] Xinyi Liu,[1,2] Nana Zhang,[3,6] Lei Shi,[1] Cheng-Feng Qin,[3,*] and Zhiheng Xu[1,4,*]

[1]State Key Laboratory of Molecular Developmental Biology, Institute of Genetics and Developmental Biology, Chinese Academy of Sciences, Beijing 100101, China
[2]University of Chinese Academy of Sciences, Beijing 100101, China
[3]Department of Virology, State Key Laboratory of Pathogen and Biosecurity, Beijing Institute of Microbiology and Epidemiology, Beijing 100071, China
[4]Parkinson's Disease Center, Beijing Institute for Brain Disorders, Beijing 100101, China
[5]Institute of Life Sciences, Fuzhou University, Fuzhou 350116, China
[6]Guangxi Medical University, Nanning 530021, China
[7]Co-first author
*Correspondence: qincf@bmi.ac.cn (C.-F.Q.), zhxu@genetics.ac.cn (Z.X.)

SUMMARY

The link between Zika virus (ZIKV) infection and microcephaly has raised urgent global alarm. The historical African ZIKV MR766 was recently shown to infect cultured human neural precursor cells (NPCs), but unlike the contemporary ZIKV strains, it is not believed to cause microcephaly. Here we investigated whether the Asian ZIKV strain SZ01 could infect NPCs in vivo and affect brain development. We found that SZ01 replicates efficiently in embryonic mouse brain by directly targeting different neuronal linages. ZIKV infection leads to cell-cycle arrest, apoptosis, and inhibition of NPC differentiation, resulting in cortical thinning and microcephaly. Global gene expression analysis of infected brains reveals upregulation of candidate flavirus entry receptors and dysregulation of genes associated with immune response, apoptosis, and microcephaly. Our model provides evidence for a direct link between Zika virus infection and microcephaly, with potential for further exploration of the underlying mechanisms and management of ZIKV-related pathological effects during brain development.

INTRODUCTION

Recent world attention has been drawn to a global Zika virus (ZIKV) outbreak and its link with devastating cases of microcephaly. ZIKV infection is spreading rapidly within the Americas after originating from an outbreak in Brazil. So far 31 countries and territories in South and Central America have reported the circulation of this type of mosquito-borne flavivirus (Heukelbach et al., 2016). There is mounting concern about the association of ZIKV infection with approximately 5,000 fetal and newborn microcephaly cases and with serious neurological complications in adults, such as Guillain-Barré syndrome. In November 2015, the Brazilian Ministry of Health reported a 20-fold increase in cases of neonatal microcephaly, which corresponds geographically and temporally to the ZIKV outbreak (Marrs et al., 2016). Due to this global threat, WHO declared a public health emergency of international concern on February 1 (Heymann et al., 2016; Marrs et al., 2016).

Precise timing of proliferation/self-renewal of neural progenitor cells (NPCs) and of their differentiation, neuronal migration, and maturation are essential for normal mammalian brain development. Disturbance of these processes leads to developmental brain disorders including microcephaly (Kriegstein and Alvarez-Buylla, 2009; Manzini and Walsh, 2011; Nowakowski et al., 2016; Thornton and Woods, 2009).

A causal association between ZIKV infection and microcephaly was proposed based on an increased incidence of microcephaly coinciding with the ZIKV outbreak and the detection of ZIKV in both microcephalic fetal brain tissues and the amniotic fluid of pregnant women with microcephalic fetuses (Calvet et al., 2016; Driggers et al., 2016; Marrs et al., 2016; Mlakar et al., 2016). In addition, ZIKV strain MR766 has been shown to be capable of infecting NPCs derived from human induced pluripotent stem cells (hiPSCs) (Tang et al., 2016). ZIKV infection induces cell death and deregulation of cell-cycle progression of hiPSCs, reducing their viability and growth as neurospheres and brain organoids (Garcez et al., 2016; Tang et al., 2016, Qian et al., 2016). However, there is still an urgent demand for direct evidence from mammalian animal models that ZIKV infection can cause microcephaly. Here we used an Asian ZIKV strain, SZ01, isolated from a patient infected in Samoa (Deng et al., 2016) to investigate whether ZIKV infects the embryonic mouse brain and affects brain development.

RESULTS

ZIKV Replicates Efficiently in Embryonic Mouse Brain and Causes Microcephaly

To test whether the contemporary ZIKV strain can infect the embryonic mouse brain, different titers of ZIKV SZ01 or culture medium (mock) were injected into one side of the cerebroventricular space/lateral ventricle (LV) of embryonic day 13.5 (E13.5)

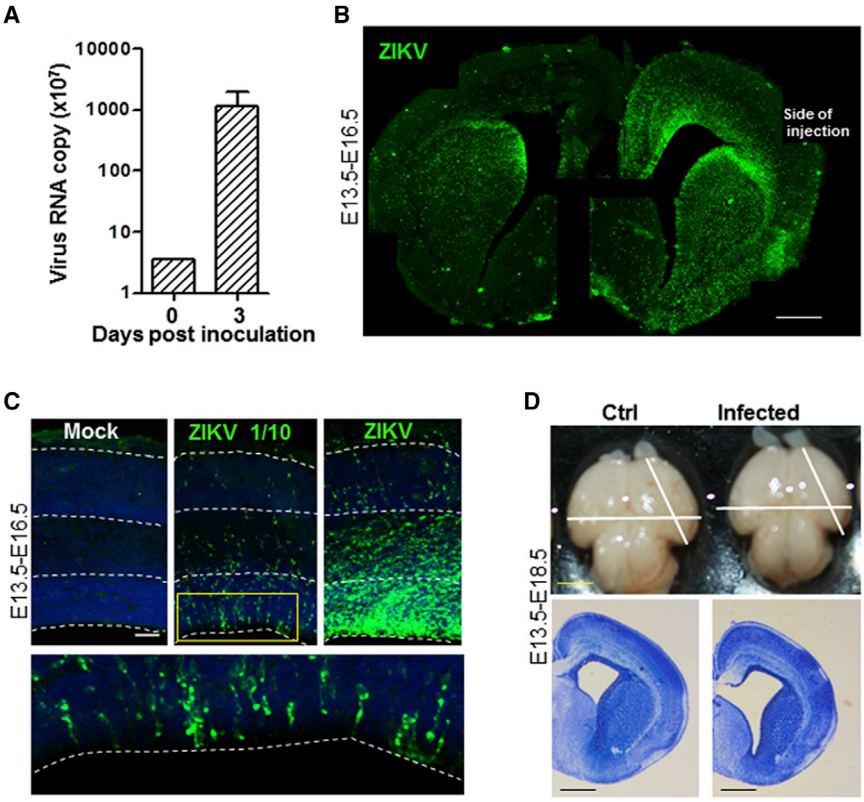

Figure 1. ZIKV Replicates Efficiently in Embryonic Mouse Brain and Causes Microcephaly

(A) Viral RNA copies were determined by real-time RT-PCR of whole brains. Data are means ± SEM from two independent experiments.

(B–D) Embryonic brains were injected with ZIKV in the lateral ventricle at E13.5 and inspected at E16.5 (B and C) or E18.5 (D). (B) Coronal section of a whole brain slice stained with ZIKV serum. Scale bar, 400 μm. (C) Images of coronal sections stained with DAPI to label nuclei (blue) and ZIKV antiserum (green). Left: mock-infected (control), middle: 1/10 diluted, right: undiluted virus. Lower panel: High-magnification of the area outlined by the yellow box. Scale bar, 40 μm. (D) Images of E18.5 infected or mock-infected littermate brains. Lower panel: similar position of coronal sections of cortices with Nissl staining. Scale bar, 5 mm (upper panel), 1 mm (lower panel).

See also Figure S1.

littermate brains and inspected 3 or 5 days later. Infection of the embryonic brains was verified by real-time PCR and with immunocytochemistry. The brains were readily infected since an ~300-fold increase of viral RNA copies was detected 3 days after infection (Figure 1A). Convalescent serum from a ZIKV-infected patient was used for immunocytochemistry staining and co-stained well with ZIKV envelope antibody (Figure S1). The numbers of ZIKV-infected cells corresponded to the amount of virus applied, with most of the infected cells located in the ventricular and subventricular zones (VZ and SVZ), where NPCs are located (Figures 1B and 1C). There were far fewer infected cells in the midbrain or the cortical plate (CP), where post-mitotic neurons are located during the infection window. Together with the random diffusion of virus injected in the LV, this may account for the variability of the infection pattern in Figure 1B.

Importantly, brains of smaller sizes compared to those of their mock infected littermates were detected 5 days after infection (Figure 1D). In addition, we noticed enlarged LVs and a thinner CP and VZ/SVZ in the infected brains (Figures 1D and 2A). We also stained the cortex with different cortical layer markers at E18.5, including Tbr1 and Foxp2, and found that ZIKV infection led to a thinning of cortical layers without apparent disturbance of the lamination (Figures 2A–2C). We were also interested in examining postnatal stages to confirm that viral infection of SZ01 leads to microcephalic brains. Unfortunately, we tried twice to infect and mock-infect littermates at E13.5 and found that the infected newborn pups were eaten by their lactating mothers within 2 days. This prevents the analysis of postnatal stages for the time being, and we therefore focused on analyzing infected brains at embryonic stages in the present study.

ZIKV Infects NPCs and Causes Cell Death

Increased cell death has been shown as one of the causes of microcephaly (Xu et al., 2014). In order to determine whether cell death contributes to the smaller size of infected brains, we infected or mock-infected littermate brains at E13.5 and inspected them 3 or 5 days later. Compared to mock-infected brains, many cells in the intermediate zone (IZ) and CP were strongly positive for the activated form of caspase3 3 days after infection, although a weak signal was also detected in the SVZ (Figure S2A). Interestingly, there were many more strongly positive cells 5 days after infection and these were mostly located in the CP (Figures 2D). This suggests that ZIKV infection induces cell death mainly in immature neurons and mature neurons.

To identify which cell types were infected by ZIKV in the embryonic brain, we examined E16.5 brain slices with cell markers including Sox2 and Pax6, markers for apical progenitor cells and radial glial cells; Tbr2, a marker for intermediate or basal progenitor cells (IPCs/BPCs); and Tuj1 and Dcx, markers for immature neurons. As shown in Figures 3A and S3, infected cells were positive for Sox2, Pax6, or Tbr2, suggesting that ZIKV mainly infects NPCs or IPCs/BPCs. Some infected cells were also positive for Tuj1 or Dcx in the IZ and CP, which had possibly differentiated from NPCs infected earlier (Figures 3B and S3C). Together, these results establish that NPCs in the developing brain are the main direct targets of ZIKV. However, almost all cells in the brain including those in the CP were also positive for ZIKV 5 days after infection (Figures 2B–2D and S2B), indicating that post-mitotic neurons can also be the target of ZIKV.

ZIKV Infection Leads to Dysregulation of NPC Cell Cycle and Differentiation

We went on to determine whether ZIKV infection would affect NPC proliferation and differentiation. It was interesting to notice that there were significantly fewer mitotic cells in the VZ of the E16.5 brains infected at E13.5 (Figure S3E). This was

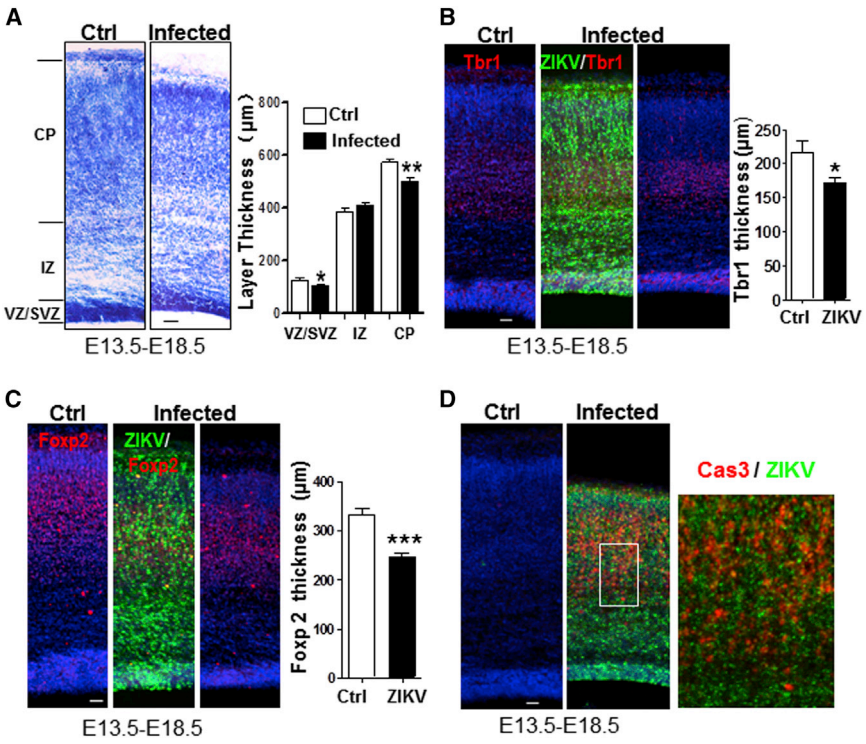

Figure 2. ZIKV Infection Leads to Thinner Cortex and Increased Cell Death

Embryonic littermate brains were infected at E13.5 and inspected at E18.5.

(A) Nissl staining of infected and mock-infected cortices. Right panel: quantification of layer thickness. Ctrl and Infected: n = 12. n: brain slices in two controls or three ZIKV-infected brains.

(B and C) Images of cortices stained for Tbr1 (B) or Foxp2 (C) and ZIKV (green). Right panels: quantification of thickness measured with individual markers. Ctrl: n = 5. Infected: n = 7. n: brain slices in two controls or six ZIKV-infected brains.

(D) Coronal sections of cortices stained with the activated form of caspase3 (Cas3, red) and ZIKV (green). Right panel: high magnification of the area outlined by the white box.

All data are means ± SEM, t test. *$p < 0.05$, **$p < 0.01$, ***$p < 0.001$. All scale bars, 40 μm. See also Figure S2.

accompanied by more centrosomes at the ventricular surface that were facing away from the nuclei. We therefore examined phosphorylated H3, a marker for cells in the M phase. As shown in Figure 3C, there were substantially fewer cells positive for phosphorylated H3 in the VZ/SVZ of ZIKV-infected brains, indicating a decreased number of NPCs in M phase. In addition, more $Pax6^+$ cells were found in infected brains 1 hr after BrdU injection, while significantly fewer $Tbr2^+$ cells were found 24 hr after BrdU injection (Figures 3D and S3D). Intriguingly, 24 hr after BrdU labeling, the infected cells positive for Ki67 or BrdU were more concentrated in the VZ (Figure 3E). Furthermore, most of the infected cells in the VZ showed the morphology of S, G1, or G2 phase cells with the somas away from the ventricular surface but tethered there through elongated end-feet (Figure 1C). Finally, the percentage of cells in the infected brains positive for both Ki67 and BrdU was increased after 24 hr of BrdU labeling (Figure 3E), suggesting that ZIKV infection inhibits NPC cell-cycle exit and differentiation. The above results indicate that ZIKV infection suppresses NPC proliferation, the transition of $Pax6^+$ radial glial cells to $Tbr2^+$ IPCs, and NPC differentiation. They are in agreement with the finding that ZIKV infection leads to S phase arrest of hiPSCs (Tang et al., 2016) and that proliferating NPCs exhibit a much longer S phase than those committed to neuronal differentiation (Arai et al., 2011).

ZIKV Infection Induces Immune Response and Deregulation of Microcephaly-Associated Genes

To investigate the global impact of ZIKV infection on the whole developing brain at the molecular level, we carried out global transcriptome analyses (RNA-seq). Genome-wide analyses identified a large number of differentially expressed genes at 3 days after viral infection (Table S2). Gene Ontology analyses revealed a particular enrichment of upregulated genes in immune-response-related and apoptosis pathways (Figure 4A and Table S2). Very notable were the genes related to cytokine production and the response to cytokines, suggesting that cytokines play a critical role in the pathogenesis of ZIKV infection (Figure 4A and Table S2). Many antiviral response genes were reported to be induced by ZIKV in human skin fibroblasts (Hamel et al., 2015). Although there is a much longer list of related genes in our dataset, we have confirmed all of those reported by Hamel et al., including Tlr3, Ddx58, Ifih1, Oas2, Isg15, and Mx1, in addition to Ccl5, Cxcl10, and Ifnb1, which were not detected in controls but were expressed in infected brains (Figure 4C and Table S2). Interestingly, many candidate flavivirus entry receptors were also induced, most notably AXL, which has been predicted as a ZIKV receptor (Nowakowski et al., 2016) (Figure 4D and Table S2). In contrast, many genes involved in cell proliferation, differentiation, migration, and organ development were downregulated (Figure 4B and Table S2). It was of interest that most of the microcephaly-associated genes were significantly downregulated (Figure S4) in the dataset of ZIKV-infected hNPCs (Tang et al., 2016). We confirmed the significant downregulation of seven of them, including ASPM, CASC5, CENPF, MCPH1, RBBP8, STIL, and TBR2, in our dataset or by real-time PCR of the virus-injected sides of the brains (Figure 4E). The downregulation of microcephaly-associated genes that we found largely overlaps with that found in the hNPC dataset, although the downregulation of CEP152 and WDR62 was not very significant. Therefore, these global transcriptome datasets not only support our cell biology findings but also provide a useful resource for the exploration of the underlying pathogenesis and for the potential treatment of ZIKV infection when combined with a dataset from hiPSCs (Tang et al., 2016).

DISCUSSION

Our results demonstrate that ZIKV can directly infect different lineages of NPCs and immature neurons in vivo in the beginning

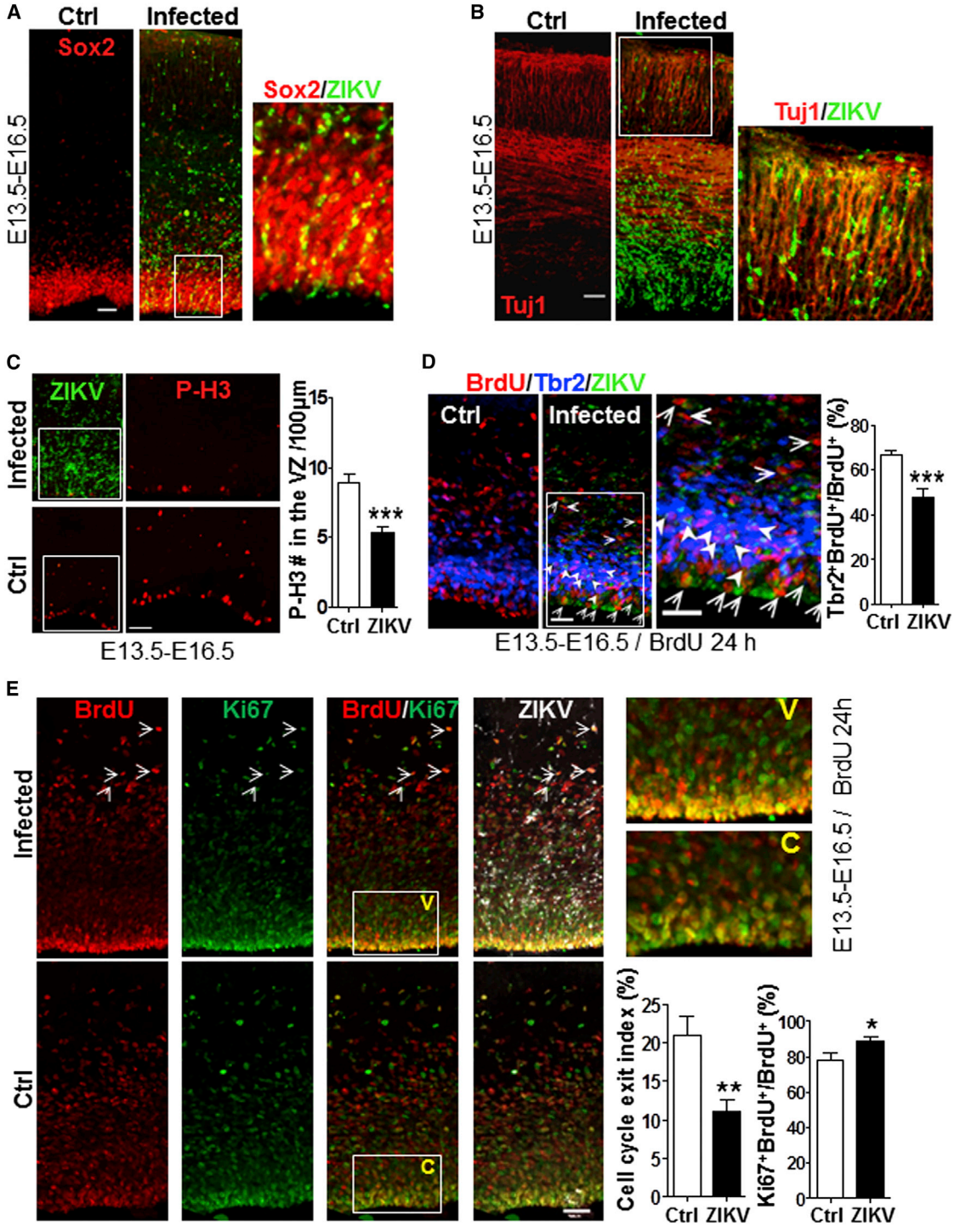

Figure 3. ZIKV Infects Different Linages of Neural Progenitor Cells

Coronal sections of E16.5 cortices infected or mock-infected at E13.5 are shown.

(A–C) Sections were stained with antibodies for Sox2 (A), Tuj1 (B), Phospho-Histone H3 (C) (red), and ZIKV (green). Right panel in (A) and (B) and middle panel in (C): high magnification of the areas outlined by the white boxes. Right panel in (C): quantification of P-H3^{+} cells in the VZ. n = 7.

(D and E) Coronal sections from infected or mock-infected E16.5 littermates 24 hr after BrdU labeling. (D) Sections were stained for ZIKV (green), Tbr2 (blue), and BrdU (red). White arrows: ZIKV and BrdU double-positive cells; arrowheads: Tbr2, BrdU, and ZIKV triple-positive cells. Right panel: quantification of Tbr2 and BrdU double-positive cells per total BrdU^{+} cells within ZIKV-positive or -negative cells (control). n = 7. (E) Sections stained for ZIKV (white), Ki67 (green), and BrdU

(legend continued on next page)

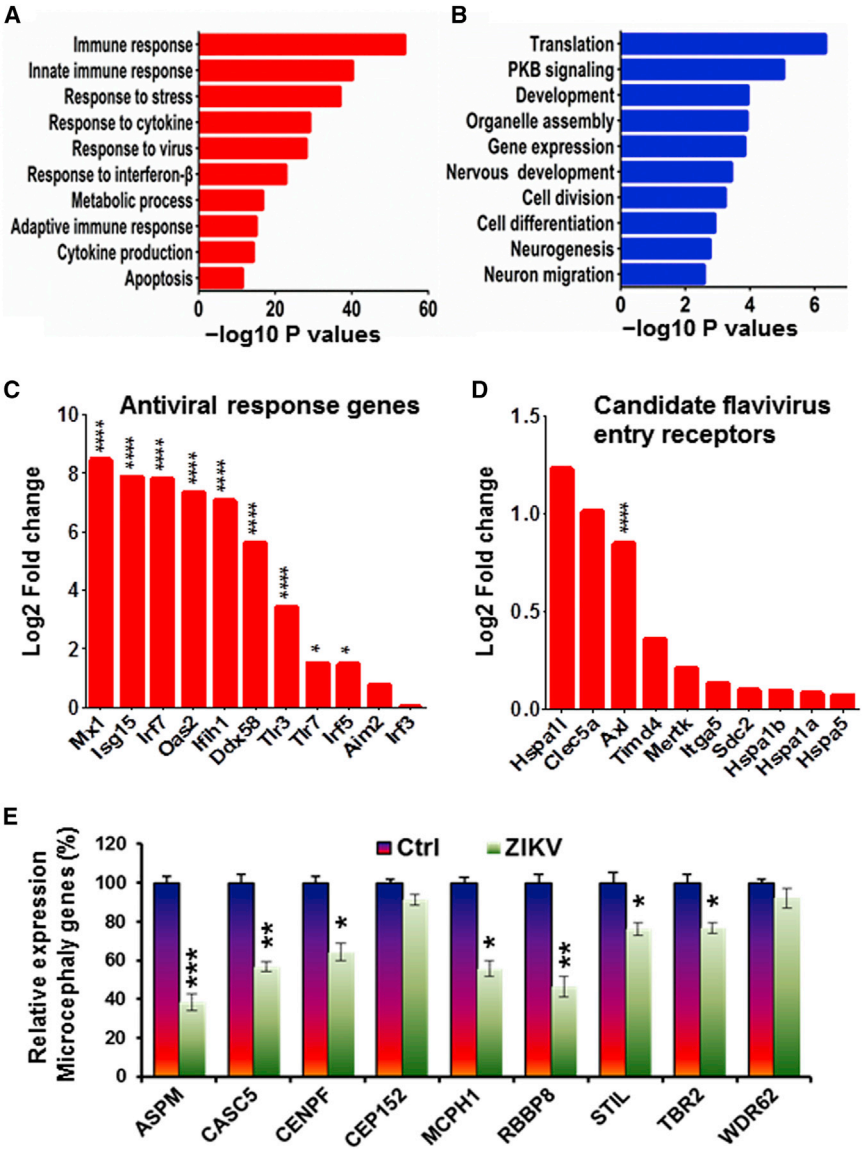

Figure 4. ZIKV Infection Causes Global Deregulation of Gene Expression

(A and B) RNA-seq analysis of whole ZIKV-infected and mock-infected littermate brains (E13.5–E16.5). Genes with significant differences in expression were subjected to GO analyses. The typical 20 most significant terms are selected for upregulated (A) and downregulated (B) genes, respectively. The −log10 p values are indicated by bar plots.

(C and D) RNA expression analysis of RNA-seq results in Table S2. Bar plots indicate induction of antiviral response genes (C) or the candidate flavivirus entry receptors (D) in the ZIKV-infected brains.

(E) Expression of microcephaly-associated genes between viral injection side of brains and controls as determined by real-time PCR.

All data are means ± SD. *p < 0.05, **p < 0.01, ***p < 0.005, ****p < 0.0001. See also Figure S4 and Table S2.

of infection and replicates in these cells with high efficiency. Due to the dramatically higher level of ZIKV several days after infection, neurons are also targeted at E18.5, indicating that neurons are infected at much lower efficiency than NPCs. Infection of NPCs leads to attenuated NPC expansion through virally induced apoptosis and cell-cycle dysregulation. Together with ZIKV's effects on NPC differentiation, these effects are likely to account for microcephaly in human fetuses or newborn babies. Our study also indicates that more attention should be focused on NPCs and immature neurons regarding the roles of these cells in ZIKV-associated neuropathology. It was unfortunate that our infected pups did not survive for a long time after birth. It is very likely that they were eaten by their lactating mothers because they were very sick. Therefore, in the future it will be desirable to lower the titer of ZIKV infection to determine whether the pups will survive longer, because if they do, it will permit determination of the long-term consequences of ZIKV infection. It will also be intriguing to investigate whether ZIKV infects adult neural stem cells and affects adult neurogenesis.

In summary, our results show direct effects of ZIKV on NPC development, including proliferation, differentiation, and cell death, which may link ZIKV with the development of microcephaly. Our study also provides insights into indirect effect of ZIKV infection on induced immune responses, including cytokine production and the effects of these cytokines on neural development. Moreover, the combination and comparison of our global transcriptome datasets of infected brains with that of hiPSCs (Tang et al., 2016) will provide valuable resources for further investigation of the underlying cellular and molecular mechanisms and management of ZIKV-related pathological effects during neural development.

EXPERIMENTAL PROCEDURES

ZIKV Preparation and Animal Infection

1 μl of ZIKV SZ01 (GenBank accession number: GEO: KU866423) virus stock (6.5×10^5 PFU/ml) (Deng et al., 2016) or stock diluted 10-fold was injected into one side of the cerebroventricular space/LV of the E13.5 ICR mouse brains and inspected 3–5 days later or after birth. Diluted virus was used only in Figure 1A

(red). Right upper panel: high magnification of the area outlined by the white box. Right lower panels: quantification of cell-cycle exit index ($Ki67^-BrdU^+/BrdU^+$) (n = 12) and $Ki67^+BrdU^+$ cells in BrdU-labeled cells within ZIKV-infected or uninfected control cells (n = 9). Arrows: $Ki67^+BrdU^+$ in ZIKV-infected cells.

All data are means ± SEM; *p < 0.05, **p < 0.01, ***p < 0.001. n: brain slice numbers from four or five different ZIKV or control littermate brains. All scale bars, 40 μm. See also Figure S3.

while all others were undiluted. For each pregnant dam, around two-thirds of littermates were injected with ZIKV while one-third were injected with culture medium (mock) for proper controls. For BrdU labeling experiments, pregnant dams were injected with 50 mg/kg (body weight) of BrdU in solution at either 1 hr or 24 hr before scarification. All experimental procedures involved were performed according to protocols approved by the Institutional Animal Care and Use Committee at Beijing Institute of Microbiology and Epidemiology.

Immunohistochemistry and Antibodies

For cryosections, tissues were fixed in 4% PFA, dehydrated in 30% sucrose, and frozen in TFM (tissue freezing medium). Sections (thickness: E16.5, 50 μm; E18.5, 40 μm) were used for immunofluorescence staining as described previously (Xu et al., 2014; Zhang et al., 2014). The antibodies used for immunostaining were Sox2 (Abcam, ab97959, 1:1000), Pax6 (Covance, PRB-278P, 1:1000), Tbr2 (Millipore, ab15894, 1:1000), β-III Tubulin (Abcam, ab7751, 1:1000), γ-Tubulin (Abcam, ab11316, 1:1000), Phospho-Histone 3 (P-H3) (Abcam, ab10543, 1:1000), Ki67 (Abcam, ab15580, 1:1000), BrdU (Abcam, ab6326, 1:500), Activated-caspase3 (CST, 9664s, 1:500), Dcx (CST, 4604s, 1:1000), Tbr1 (Abcam, ab31940, 1:500), Foxp2 (Abcam, ab16046, 1:500), and ZIKV serum from a patient (1:100). Control serum for ZIKV was from a healthy person (1:100), and mouse serum immunized with recombinant ZIKV envelope (E) protein was from GenBank (GEO: JN860885) (1:500, used only in Figure S1B). Nuclei were stained with DAPI (Invitrogen). Sections stained for BrdU detection were subject to 10 min 1N HCl on ice and 30 min 2N HCl at 37°C prior to blocking.

Nissl Staining

Brian slices were stained with 0.1% toluidine blue for 20 min and dehydrated in turn by 70%, 96%, and 99% ethanol (45 s, twice for each). Finally, slices were hyalinized by Xylene for more than 30 min.

Confocal Imaging and Quantification

Slices were imaged on an LSM 700 (Carl Zeiss) confocal microscope, and the images were analyzed with Imaris, ImageJ, and Photoshop as described previously (Xu et al., 2014; Zhang et al., 2014). All data were analyzed using Prism software (GraphPad) or Excel. Statistical evaluation was performed by Student's unpaired t test. Data are presented as mean ± SEM.

RNA-Seq Analyses

Whole E16.5 brains 3 days after ZIKV or mock infection (two for each group) were used for global transcriptome analysis by Annoroad Co. Significantly differentially expressed genes were identified when we compared Normalized Reads Count between ZIKV and mock infection groups with $p < 0.05$ and $|\text{Log2FoldChange}| > 0.263$. Significance of Gene Ontology term enrichment was estimated with Fisher's Exact Test (p value).

Real-Time PCR

For viral RNA copies: total RNA was extracted from whole embryo brains and viral RNA copies were determined by real-time PCR (Johnson et al., 2005). Primers and fluorogenic probes for ZIKV detection were shown in Table S1. 2 μl of RNA samples was mixed with each primer of a final concentration of 0.2 μM to prepare the reaction mixtures in accordance with the One Step PrimeScript RT-PCR Kit instructions, and they were moved to a reverse transcription reaction at 42°C for 5 min, followed by PCR amplification using a 60°C annealing temperature for 40 cycles. The standard curve of viral RNA copies was determined from 10-fold dilutions of ZIKV RNA with known concentrations, and viral RNA copies in embryo brains were calculated.

Determining expression of microcephaly-associated genes between viral injection side of the brains and mock-infected control (E13.5–16.5) was performed as described previously (Xu et al., 2014), and primers used are listed in Table S1.

SUPPLEMENTAL INFORMATION

Supplemental Information for this article includes four figures and two tables and can be found with this article online at http://dx.doi.org/10.1016/j.stem.2016.04.017.

AUTHOR CONTRIBUTIONS

Z.X. and C.-F.Q. conceived of the research and Z.X. designed the study and wrote the manuscript. D.X., C.L., and S.H. designed and performed most of the experiments. Q.Y. performed ZIKV real-time PCR assays and took care of the mice. Y.J. did bioinformatics analysis. X.L. did Nissl staining. Everyone contributed to the writing.

ACKNOWLEDGMENTS

We thank Drs. Fu Gao, Xia Jin, Weixiang Guo, Lloyd Greene, and Feng Zhang for valuable advice, and we thank Fu-Chun Zhang for serum from the ZIKV patient. This work was supported by grants from NSF (China) (31430037/31271156/81522025/8151101191) and the MOST (China) "973" program (2014CB942801/2013DFA31990/2012YQ03026006).

Received: April 15, 2016
Revised: April 25, 2016
Accepted: April 29, 2016
Published: May 11, 2016

REFERENCES

Arai, Y., Pulvers, J.N., Haffner, C., Schilling, B., Nüsslein, I., Calegari, F., and Huttner, W.B. (2011). Neural stem and progenitor cells shorten S-phase on commitment to neuron production. Nat. Commun. *2*, 154.

Calvet, G., Aguiar, R.S., Melo, A.S., Sampaio, S.A., de Filippis, I., Fabri, A., Araujo, E.S., de Sequeira, P.C., de Mendonça, M.C., de Oliveira, L., et al. (2016). Detection and sequencing of Zika virus from amniotic fluid of fetuses with microcephaly in Brazil: a case study. Lancet Infect. Dis. S1473-3099(16)00095-5. http://dx.doi.org/10.1016/S1473-3099(16)00095-5.

Deng, Y.Q., Zhao, H., Li, X.F., Zhang, N.N., Liu, Z.Y., Jiang, T., Gu, D.Y., Shi, L., He, J.A., Wang, H.J., et al. (2016). Isolation, identification and genomic characterization of the Asian lineage Zika virus imported to China. Sci. China Life Sci. *59*, 428–430, http://dx.doi.org/10.1007/s11427-016-5043-4.

Driggers, R.W., Ho, C.Y., Korhonen, E.M., Kuivanen, S., Jääskeläinen, A.J., Smura, T., Rosenberg, A., Hill, D.A., DeBiasi, R.L., Vezina, G., et al. (2016). Zika Virus Infection with Prolonged Maternal Viremia and Fetal Brain Abnormalities. N. Engl. J. Med. http://dx.doi.org/10.1056/NEJMoa1601824.

Garcez, P.P., Loiola, E.C., Madeiro da Costa, R., Higa, L.M., Trindade, P., Delvecchio, R., Nascimento, J.M., Brindeiro, R., Tanuri, A., and Rehen, S.K. (2016). Zika virus impairs growth in human neurospheres and brain organoids. Science, aaf6116, http://dx.doi.org/10.1126/science.aaf6116.

Hamel, R., Dejarnac, O., Wichit, S., Ekchariyawat, P., Neyret, A., Luplertlop, N., Perera-Lecoin, M., Surasombatpattana, P., Talignani, L., Thomas, F., et al. (2015). Biology of Zika Virus Infection in Human Skin Cells. J. Virol. *89*, 8880–8896, http://dx.doi.org/10.1128/JVI.00354-15.

Heukelbach, J., Alencar, C.H., Kelvin, A.A., De Oliveira, W.K., and Pamplona de Góes Cavalcanti, L. (2016). Zika virus outbreak in Brazil. J. Infect. Dev. Ctries. *10*, 116–120.

Heymann, D.L., Hodgson, A., Sall, A.A., Freedman, D.O., Staples, J.E., Althabe, F., Baruah, K., Mahmud, G., Kandun, N., Vasconcelos, P.F., et al. (2016). Zika virus and microcephaly: why is this situation a PHEIC? Lancet *387*, 719–721.

Johnson, B.W., Russell, B.J., and Lanciotti, R.S. (2005). Serotype-specific detection of dengue viruses in a fourplex real-time reverse transcriptase PCR assay. J. Clin. Microbiol. *43*, 4977–4983.

Kriegstein, A., and Alvarez-Buylla, A. (2009). The glial nature of embryonic and adult neural stem cells. Annu. Rev. Neurosci. *32*, 149–184.

Manzini, M.C., and Walsh, C.A. (2011). What disorders of cortical development tell us about the cortex: one plus one does not always make two. Curr. Opin. Genet. Dev. *21*, 333–339.

Marrs, C., Olson, G., Saade, G., Hankins, G., Wen, T., Patel, J., and Weaver, S. (2016). Zika Virus and Pregnancy: A Review of the Literature and Clinical Considerations. Am. J. Perinatol. http://dx.doi.org/10.1055/s-0036-1580089.

Mlakar, J., Korva, M., Tul, N., Popović, M., Poljšak-Prijatelj, M., Mraz, J., Kolenc, M., Resman Rus, K., Vesnaver Vipotnik, T., Fabjan Vodušek, V., et al. (2016). Zika Virus Associated with Microcephaly. N. Engl. J. Med. *374*, 951–958.

Nowakowski, T.J., Pollen, A.A., Di Lullo, E., Sandoval-Espinosa, C., Bershteyn, M., and Kriegstein, A.R. (2016). Expression Analysis Highlights AXL as a Candidate Zika Virus Entry Receptor in Neural Stem Cells. Cell Stem Cell. S1934-5909(16)00118-1. http://dx.doi.org/10.1016/j.stem.2016.03.012.

Qian, X., Nguyen, H.N., Song, M.M., Hadiono, C., Ogden, S.C., Hammack, C., Yao, B., Hamersky, G.R., Jacob, F., Zhong, C., et al. (2016). Brain-Region-Specific Organoids Using Mini-bioreactors for Modeling ZIKV Exposure. Cell, in press. Published online April 21, 2016. http://dx.doi.org/10.1016/j.cell.2016.04.032.

Tang, H., Hammack, C., Ogden, S.C., Wen, Z., Qian, X., Li, Y., Yao, B., Shin, J., Zhang, F., Lee, E.M., et al. (2016). Zika Virus Infects Human Cortical Neural Progenitors and Attenuates Their Growth. Cell Stem Cell. S1934-5909(16)00106-5. http://dx.doi.org/10.1016/j.stem.2016.02.016.

Thornton, G.K., and Woods, C.G. (2009). Primary microcephaly: do all roads lead to Rome? Trends Genet. *25*, 501–510.

Xu, D., Zhang, F., Wang, Y., Sun, Y., and Xu, Z. (2014). Microcephaly-associated protein WDR62 regulates neurogenesis through JNK1 in the developing neocortex. Cell Rep. *6*, 104–116.

Zhang, F., Xu, D., Yuan, L., Sun, Y., and Xu, Z. (2014). Epigenetic regulation of Atrophin1 by lysine-specific demethylase 1 is required for cortical progenitor maintenance. Nat. Commun. *5*, 5815.